# Structure Inversions in Structure-Dependent Coordinates

J. M. Joel Ong[1 2 *] Willem Hoogendam[1] Sarbani Basu[3]

[1]Institute for Astronomy, University of Hawai'i; [2]NASA Hubble Fellow [3]Yale University
[*]joelong@hawaii.edu

# We present techniques for performing structure inversions parameterised by the **acoustic** and **buoyant** radial coordinates.

## Motivation: Natural Coordinates

Structural and dynamical perturbations to a star perturb its normal-mode frequencies through integral expressions that may be written in the form

$$\delta\omega_i \sim \sum_k \int K_{i,k}(r)\ \delta f_k(r)\ \mathrm{d}r. \tag{1}$$

However, the sensitivity of these response kernels is not uniformly distributed with respect to the physical radial coordinate, $r$.

Ong et al. (2024) showed that, for rotational kernels in particular, one might uniformly redistribute the sensitivity of these kernels by transforming to a **structure-dependent coordinate system**.

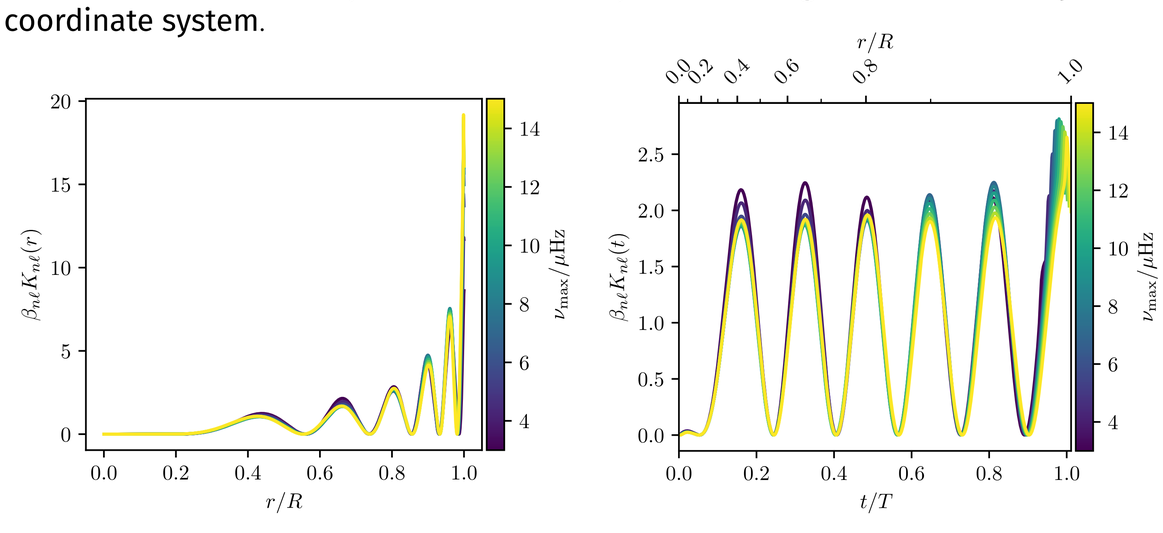


Figure 1: Redistribution to uniform sensitivity by a coordinate transformation, demonstrated using rotational kernels for the $\ell = 1, n = 6$ p-mode of a series of red-giant stellar models. The left panel shows these kernels as parameterised by the physical radial coordinate, as in eq. (1). The right panel shows these same kernels, but rescaled for integration against the acoustic radial coordinate, eq. (2). From Ong et al. (2024).

There are **two** natural coordinate systems that may be used for this purpose, depending on the character of the mode under consideration.

- For **p-modes**, we may use the **acoustic** radial coordinate:

$$t(r) = \int_0^r \frac{\mathrm{d}r'}{c_s}. \tag{2}$$

- For **g-modes**, we may use the **buoyant** radial coordinate:

$$b(r) = \int_{r_1}^r \frac{|N|}{r}\mathrm{d}r. \tag{3}$$

Ong et al. (2024) successfully applied this technique to **rotational** inversion. Can we do the same for inversions for **stellar structure**?

## Lagrangian vs. Eulerian Kernels

Consider two stellar structures — a "reference" structure with sound-speed profile $c_1(r)$, and a "target" structure with sound-speed profile $c_2(r)$. The standard set of inversion kernels in eq. (1) relate frequency perturbations $\delta\omega$ to **Eulerian** structural differences: e.g.

$$\delta c(r) = c_2(r) - c_1(r) \tag{4}$$

where differences are taken **at the same physical radius** in both the reference and target structure. Homology transformations may permit rescaling to e.g. matching *fractional* physical radius, instead.

Conversely, we define the **Lagrangian** structural differences as being differences taken at the **same value of the structure-dependent coordinate**. For example:

$$\delta\tilde{c}(t) = c_2(t_2^{-1}(t)) - c_1(t_1^{-1}(t)). \tag{5}$$

The two are related as

$$\delta\tilde{c}(t(r)) = \delta c(r) - \frac{\mathrm{d}c}{\mathrm{d}t}\int \frac{\delta t(r)}{\delta c(r')}\delta c(r')\mathrm{d}r' \tag{6}$$

The second term — with an integral taken over a functional derivative — is required to describe contributions to $\delta\tilde{c}(t(r))$ arising from perturbations to $c(r)$ modifying $t(r)$ itself.

*[ Compare this with how Eulerian $f'$ and Lagrangian $\delta f$ are related as $\delta f = f' + \boldsymbol{\xi}\cdot\nabla f$ ]*

This in turn means that the kernels for Lagrangian sound-speed differences, $\tilde{K}_c$, are related to the Eulerian kernels $K_c$ of eq. (1) as

$$K_c(r) = \frac{\mathrm{d}t}{\mathrm{d}r}\tilde{K}_c(t(r)) - \int \frac{\mathrm{d}c}{\mathrm{d}t}(r')\frac{\delta t(r')}{\delta c(r)}\left(\frac{\mathrm{d}t}{\mathrm{d}r}\tilde{K}_c(t(r'))\right)\ \mathrm{d}r'\ . \tag{7}$$

Solving for $\tilde{K}_c$ from eq. (7) (a Volterra integral equation) is not trivial, but may be done numerically. More general expressions (summing over indepedent perturbations) are required to construct cross-term kernels, e.g. $\tilde{K}_{\rho,c_s}$.

## Numerical Results: p-modes

We implement solutions to eq. (7) using the method of Neumann series, accelerated using `jax` (Bradbury et al., 2018), shown applied to the $c_s^2, \rho$ kernel pair in fig. 2. Moreover, the functional derivative in eq. (7) may be constructed either to maintain a fixed total acoustic radius, or to permit it to vary under perturbations to the sound speed.

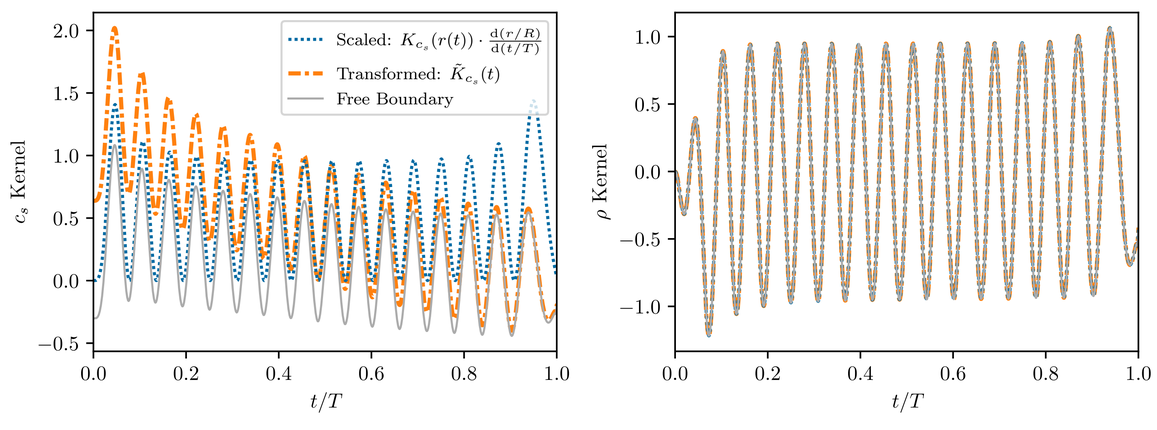


Figure 2: Lagrangian $c_s^2$ and $\rho$ kernels for the $\ell = 1, n_p = 16$ p-mode of Model S. The blue dotted curve shows the Eulerian kernels, scaled by the integral measure $\frac{\mathrm{d}r}{\mathrm{d}t} = c_s$. The orange dash-dotted curve shows solutions to eq. (7) with the functional derivative computed such that acoustic radius is unchanged by the perturbation, while the gray curve shows solutions with a free boundary.

We found that **only** the free-boundary kernels permitted Lagrangian quantities to be recovered in a mock inversion exercise — the fixed-boundary kernels have shapes that prevent OLA localisation kernels from being constructed.

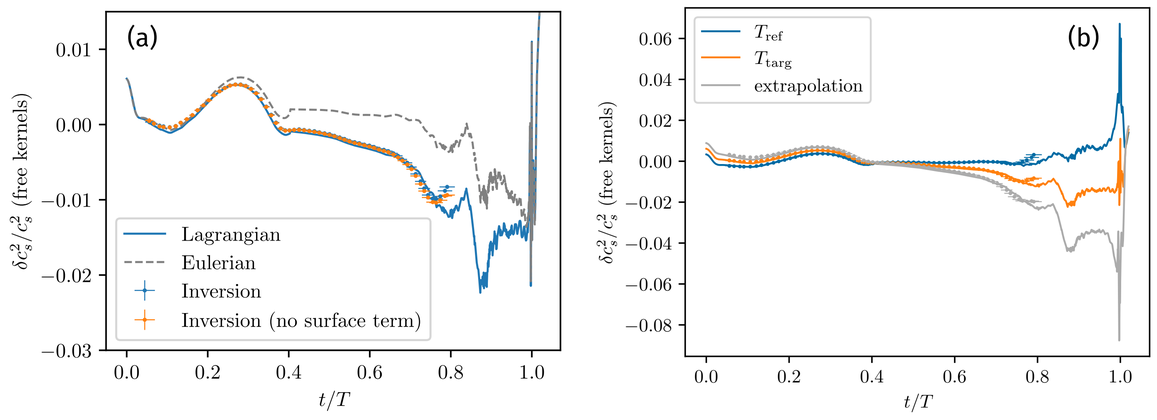


Figure 3: We successfully performed inversions for Lagrangian sound-speed differences in a model-model comparison. **(a)** OLA sound-speed inversions using our modified kernels; the recovered sound-speed differences agree better with the Lagrangian than Eulerian differences. **(b)** In order to compare stellar models with different acoustic radii, the reference model frequencies, and sound speed, had to be scaled by an assumed value of the (notionally unknown) reference acoustic radius. However, both the ground-truth and inversion results transform in the same way using different choices of this assumed acoustic radius.

## Numerical Results: g-modes

We apply eq. (7) (generalised to the buoyancy radial coordinate) to the $N^2, \rho$ kernel pair, shown in fig. 4. Unlike the Eulerian picture, the Lagrangian $N^2$ kernels are zero-mean.

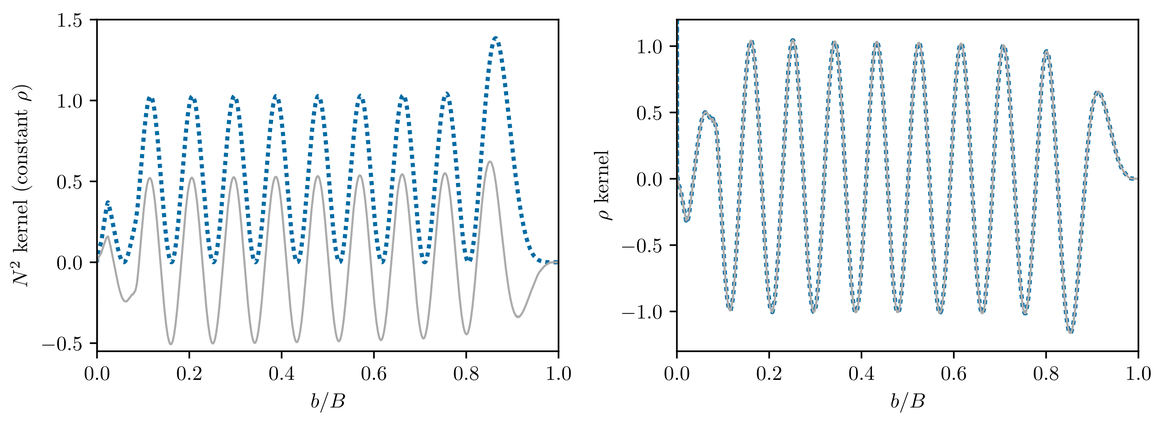


Figure 4: Lagrangian $N^2$ and $\rho$ kernels for the $\ell = 1, n_g = 10$ g-mode of the "reference" model from Vanlaer et al. (2023). Line colours and styles have the same meanings as in fig. 2.

Eulerian inversions with g-modes are plagued by nonlinear phenomena (Vanlaer et al., 2023); one symptom of this is that the kernels of the target and reference model appear different when plotted on the same axes. **This does not affect buoyancy-radius Lagrangian kernels**; they may well be the only meaningful path to g-mode inversions.

## References

Bradbury, J., Frostig, R., Hawkins, P., et al. 2018, JAX: composable transformations of Python+NumPy programs, 0.3.13. *http://github.com/google/jax*

Ong, J. M. J., Hon, M. T. Y., Soares-Furtado, M., et al. 2024, ApJ, 966, 42, doi: *10.3847/1538-4357/ad2ea2*

Vanlaer, V., Aerts, C., Bellinger, E. P., & Christensen-Dalsgaard, J. 2023, A&A, 675, A17, doi: *10.1051/0004-6361/202245597*